

Article

Design Optimization of a Permanent-Magnet Saturated-Core Fault-Current Limiter

John Linden * , Yasha Nikulshin * , Alex Friedman *, Yosef Yeshurun * and Shuki Wolfus *

Laboratory for Magnetic Measurements and Institute of Superconductivity, Department of Physics, Bar-Ilan University, Ramat-Gan 5290002, Israel

* Correspondence: lindenjhn@gmail.com (J.L.); yasha.nick@gmail.com (Y.N.); freidma@gmail.com (A.F.); yosiyeshurun@gmail.com (Y.Y.); shuki.wolfus@gmail.com (S.W.)

Received: 11 April 2019; Accepted: 10 May 2019; Published: 14 May 2019



Abstract: Designs of saturated-cores fault current limiters (FCLs) usually implement conducting or superconducting DC coils serving to saturate the magnetic cores during nominal grid performance. The use of coils adds significantly to the operational cost of the system, consuming energy, and requiring maintenance. A derivative of the saturated-cores FCL is a design implementing permanent magnets as an alternative to the DC coils, eliminating practically all maintenance due to its entirely passive components. There are, however, various challenges such as the need to reach deep saturation with the currently available permanent magnets as well as the complications involved in the assembly process due to very powerful magnetic forces between the magnets and the cores. This paper presents several concepts, achieved by extensive magnetic simulations and verified experimentally, that help in maximizing the core saturation of the PMFCL (Permanent Magnet FCL), including optimization of the permanent magnet to core surface ratios and asymmetrical placement of the permanent magnets, both creating an increase in the cores' magnetic flux at crucial points. In addition, we point to the importance of splitting the AC coils to leave the center core point exposed to best utilize their variable inductance parameters. This paper also describes the stages of design and assembly of a laboratory-scale single phase prototype model with the proposed PMFCL design recommendations, as well as an analysis of real-time results obtained while connecting this prototype to a 220 V grid during nominal and fault states.

Keywords: Fault Current Limiters; permanent magnets; saturated core; variable inductance

1. Introduction

The continuous growth of energy generation and the worldwide efforts to integrate renewable energy sources in existing grids while maintaining a high level of power quality, result in an ever-increasing need to solve the problem of fault currents [1–5]. One of the proposed solutions, already being integrated at various locations [6–8], is a saturated-cores fault current limiter (SCFCL). The SCFCL device operates in series with the electrical grid acting as a variable impedance reactor. The concept of its operation consists of keeping the magnetic cores saturated during nominal grid performance so that the AC coils, mounted on the saturated cores and connected in series with the grid, exhibit a low impedance [9]. When a fault state is experienced, the AC coils create an opposing magnetic field, overcoming the saturation bias of the magnetic cores. The impedance, being proportional to the permeability of the core, increases significantly, limiting the prospected fault current. The voltage drop across the FCL device is:

$$V_{FCL} = IR + \frac{d(LI)}{dt}, \quad (1)$$

where R is the device resistance, I the current, and L the inductance of the AC coils. The inductance is a derivation of the coil's parameters (winding density, cross section, and length), and the magnetic permeability, which depends strongly on the current, providing dynamic values to L throughout the current cycle. The dynamic inductance was shown [10] to play a major role in the effective operation of SCFCLs, since the time derivative of the dynamic inductance contributes to the FCL voltage and hence to its limiting capability.

The saturating DC coils, which are essential for the successful operation of the SCFCL, add significantly to the operational cost of the system, consuming energy and requiring maintenance. Moreover, being inductive on its own, the DC bias coil may interact with the AC grid coils through electromagnetic coupling and degrade the performances of the limiter or the power supply driving the DC coils, as well as degrading the power quality of the grid. It was therefore argued [11] that FCL designs based on permanent magnets (PMFCL), rather than electromagnets, may offer a better solution for the fault current limiters. In these designs, permanent magnets are used to provide the saturation of the core in inductive FCL devices. The main advantage of PMFCLs stems from the fact that they do not require any sensors or control devices, allowing for automatic, passive, and instantaneous limiting and recovery, as well as essentially zero maintenance.

Recently, various designs have been developed implementing permanent magnets to provide the saturation in inductive FCL devices [11–19]. These designs all incorporate permanent magnets as a means of saturating the core. While, as mentioned, the use of permanent magnets has many advantages, it also presents several new challenges. For example, in a typical saturated-cores FCL it is necessary to saturate the magnetic core, but the highest remanence of permanent magnets to date is only ~ 1.4 T. Additionally, the assembly process of the permanent magnets in the presence of iron cores proves a challenging stage because of the very powerful magnetic forces involved. It is therefore important that these fields be utilized to their maximum potential, allowing for deep nominal state saturation of the cores while using the smallest possible permanent magnets.

This paper presents several concepts that contribute to optimizing the implementation of permanent magnets to assist in overcoming these challenges. Adoption of these proposed concepts has been simulated and tested experimentally by building a low voltage prototype, and demonstrated improvements in performance as well as weight reductions of up to 20% in the permanent magnets and core materials when implemented. These concepts include the optimal permanent magnet to core ratios and asymmetrical placement of the magnets (in an otherwise symmetrical design) increasing the directional flux within the cores while minimizing residual fields and volume of materials. Splitting the AC coils in the center is also shown to benefit the nominal losses due to the magnetic profile within the cores. Other than these novel concepts, adopting a design that utilizes unidirectional flux was beneficial in terms of minimizing the core volumes and residual fields. Configurations that place the magnets with opposing directional fields create areas within the core held out of saturation throughout nominal work cycles, thus leaving areas that do not contribute to the effective inductance of the device.

In this paper, we present the design and building of a laboratory-scale single phase prototype model of the proposed PMFCL. We present an analysis of real-time results obtained while connecting this prototype to a 220 V grid during nominal and fault states.

2. Design and Optimization

The prototype design is shown in Figure 1. It utilizes N52 grade $Nd_2Fe_{14}B$ permanent magnets (shown in blue) and HiB laminated silicon steel cores (green). The orientation of the $Nd_2Fe_{14}B$ permanent magnets is such that it closes the continual magnetic circuit of the magnetic cores, creating the said unidirectional flux path. This is in contrast to designs where the DC bias source resides on a central core limb and generates DC flux that flows in a 'T' shape, splitting to clockwise and counter-clockwise directions, leaving a wasted core volume with a low DC flux.

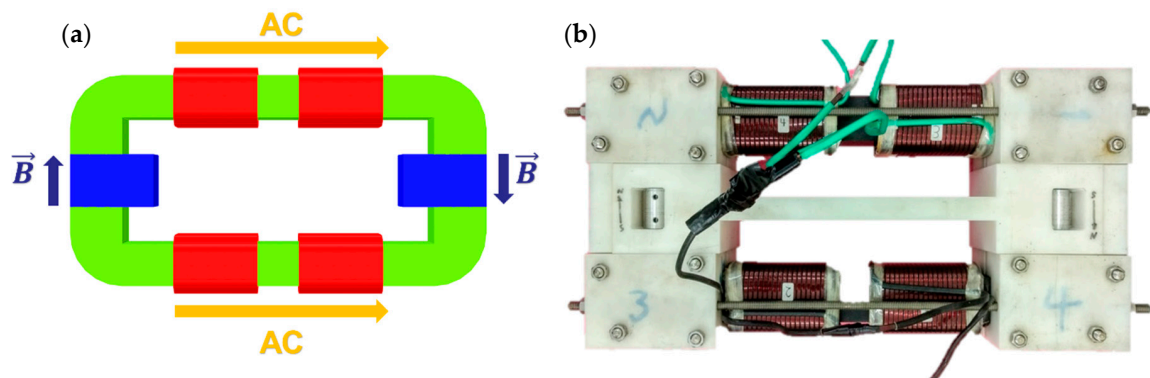


Figure 1. (a) Prototype design of PMFCL (permanent magnet fault current limiters). The left to right long yellow arrows represent the direction of the induced magnetic field due to the AC coils during one-half cycle. Green shows the Grain Oriented Silicon Steel (GOSS) core, in blue are the permanent magnets with their orientation in accordance with the direction of the black arrows. (b) The fully assembled lab-scale prototype.

In order to saturate the HiB silicon steel core, a magnetic field of $\sim 2\text{ T}$ is required. The remanence of the grade N52 magnets (as for most $Nd_2Fe_{14}B$ rare earth permanent magnets) is only $\sim 1.4\text{ T}$. To overcome this difficulty, we introduced a staged variation in the core's cross-section (see Figure 1). This has the effect of increasing the flux density from the magnets, with a larger cross-section, towards the narrower cross-sectioned core until the flux density is capable of reaching the full saturation value of the magnetic core. Figure 2 illustrated the simulated flux density map of the device. A ratio of 1:2 (core:permanent magnet) creates a flux density at the interface to sufficiently achieve saturation. A further step down in the core's cross-section in its AC limbs increases the flux density to fully achieve the required saturation. Optimization for this specific configuration was done using Cobham-Opera Simulation Software. The optimization focused on the exact dimensions and ratios of the permanent magnets to HiB GOSS (Grain Oriented Silicon Steel) cores, as shown in Figure 2, and the AC coils number of windings/dimensions, explained below as being a significant design parameter in determining the range of effective operation. Optimization of this ratio would also prove helpful for developing PMFCLs for high voltage applications [20].

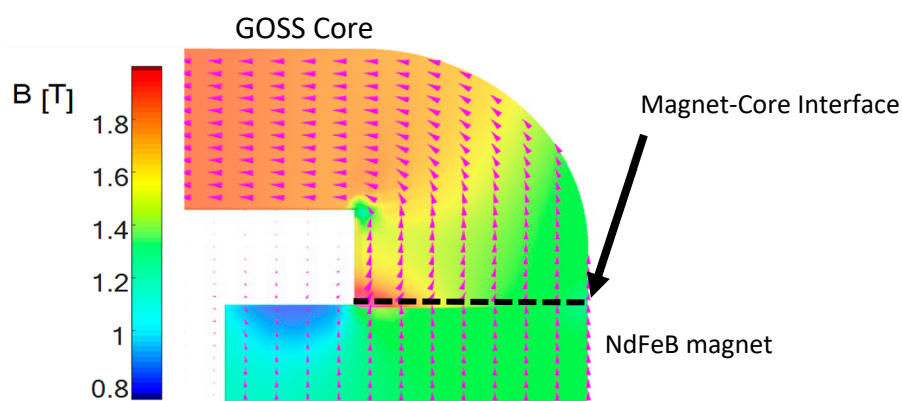


Figure 2. Magnetic flux lines of the PMFCL simulated using Opera-Vector Fields Finite Element Method (FEM) analysis. The figure is a closeup of the permanent magnet and core interface.

Two additional design features are shown in Figure 1. The first is the split in the AC coil. Following the concept described in [21], the coil is split so that the limbs' center region—where saturating field is in the core, due to its farthest distance from the permanent magnets—is minimal. Leaving this point under a lower exposure to direct AC flux helps it remain in a deeper saturated region during nominal

grid operation. Also, when the core is saturated, the separation between coil segments leads to a reduced impedance due to the weak coupling between these segments. In fault mode, when the core is desaturated, coupling increases along with the impedance. The second feature is the asymmetrical mounting of the permanent magnets, which are shifted towards the inner part of the core frame. This asymmetrical mounting contributes in reducing stray residual fields around the device (Figure 3a), and to provide further flux enhancement at the core region under the AC coils (Figure 3b). However minor these features seem, as analyzed in the results, they provide important value in enhancing the performance and efficiency when scaling up to high power PMFCLs.

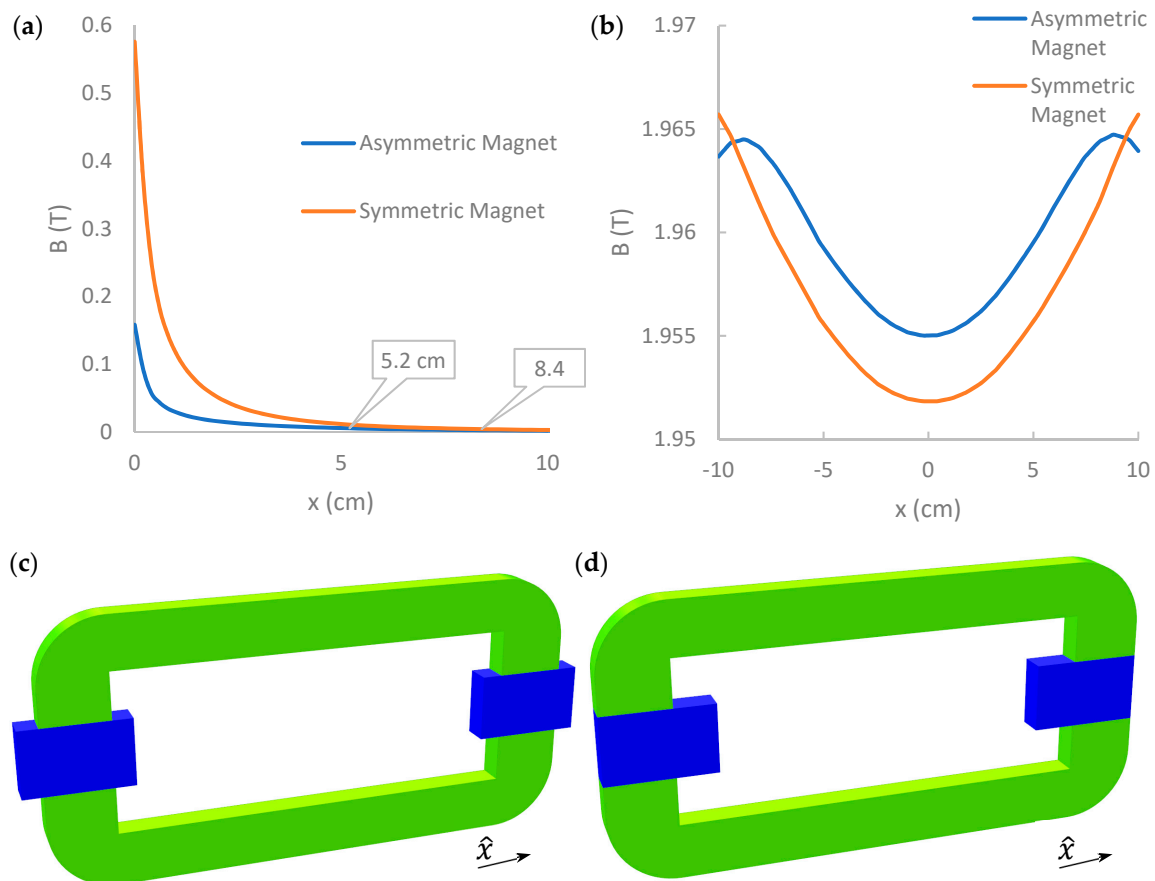


Figure 3. (a) Residual fields as a function of distance from the outer face of the permanent magnet. Simulated with symmetrically and asymmetrically placed permanent magnets. Callout points show the 0.5mT point health standards [22]. (b) Center magnetic saturation within core at the weakest point for symmetrical and asymmetrical configurations. (c) Asymmetric and (d) Symmetric illustrated configurations.

The important parameters in determining the configuration in order to obtain the desired results are as follows:

- Number of turns in AC windings, N . Both fault and insertion impedance increase with increasing N . However, $\mu(I)$ differs between both states.
- Choosing the bias point of saturation in order to optimize relation of insertion impedance to desaturation level at fault state.
- AC and DC core limb lengths—parameters which affect the level of saturation and the dimensions of the device as well as permanent magnets. Also, directly affect the inductance dependency on the current.

- Core cross section on AC side to provide improvement in flux density. Reducing the core cross-section causes the core to saturate at a lower flux bias as well as decreasing insertion and fault impedance. On the other hand, reduced core-section places the device in danger of reversed saturation during a fault, which degrades its limiting performances.
- Coil splitting, coil segment separation, and position along the AC core. As explained above, these design parameters help in improving the fault to insertion impedance ratio.
- Cross-section ratio of the permanent magnet to cores in order to hold the core in the saturated state throughout nominal cycles.

The design modeled here is appropriate for a single-phase grid, where for each half cycle the upper/lower arm is desaturated by the direction of the AC magnetic flux. Figure 4 shows the simulation results of the field intensity profile along the lower and upper AC limbs, respectively, throughout a half fault cycle. Each color in the figure represents a different point in time in the half cycle. As the waveform approaches the maximum current, at $t \rightarrow \frac{1}{4f}$, the core exits the saturation induced by the permanent magnets and reenters saturation in the reversed direction due to \vec{H} field induced by the AC coils. While the core experiences a high level of reversed saturation, these fields do not reach the permanent magnets therefore not exposing them to demagnetizing coercive fields. During the same time span, the opposite arm shown in Figure 4 shows that the saturation is held steady throughout the cycle as a result of the \vec{H}_{AC} being in the same direction as the magnetic field of the permanent magnet. The positive 'bump' evident near the center location is a result of the coil splitting feature described above. Without this split, the profile would have continued its symmetric decrease toward a minimum at $x = 0$.

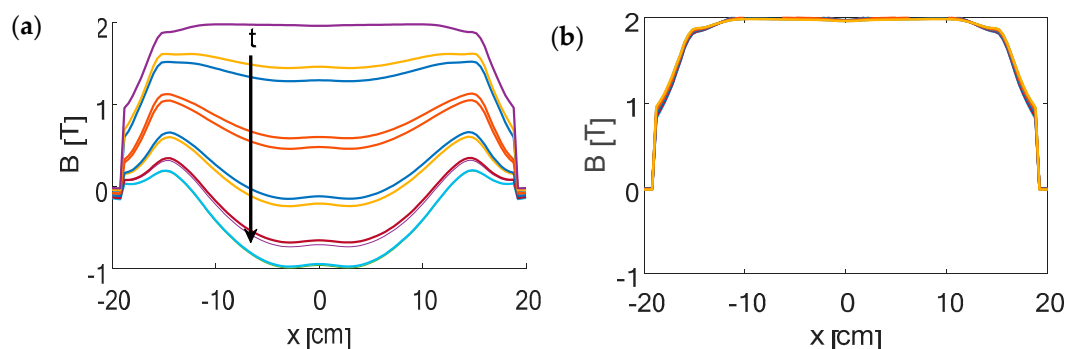


Figure 4. Magnetic field as a function of distance along the AC limb throughout a half fault cycle. (a) Lower arm during fault state. The purple line represents induction at $t = 0$. Each color in the figure represents a different time ($\Delta t = 2.5 \text{ ms}$) in the half cycle. The time flow is indicated by the arrow. (b) Induction in the upper arm during fault state at the same times as in (a).

As mentioned previously, it is important that the AC grid coils be with a center core fully saturated during nominal cycles to not introduce unwanted losses due to high permeability values in the core. This placement is achieved by analyzing the points of high saturation in the core arms, along the x axis in Figure 4 such as between -10 and 10 . The core to permanent magnet ratio does achieve its goal in increasing the flux density throughout the core, however, there still is a drop at the center point along the core in between the magnets. It would be optimal to minimize this range (graphed from -1 to 1 in Figure 4) allowing to extend the coil length in order to increase fault inductance, thus achieving higher limiting factors.

3. Assembly of Laboratory-Scale PMFCL

The attraction force between the magnet and the core, which relates to the product of $\vec{B} \cdot \frac{d\vec{B}}{dx}$ in the core, increases drastically as the distance between them decreases. In order to control the process during assembly, to both obtain proper alignment and assure no ruptures to the magnets/cores, a DC current of 100 A was introduced into the AC coils to generate an opposing magnetic flux to the permanent magnets thereby saturating the core initially and thus minimizing the product $\vec{B} \cdot \frac{d\vec{B}}{dx}$. This proved to greatly reduce the attraction forces. Coupled with a Delrin construction frame that was designed to properly align the device, these produced successful results. The magnets were initially held in place with a center Delrin block, while both cores were pulled in simultaneously with a two-way connected clamp above and below each magnet in order to hold the alignment and rotate the bolts in a single direction for tightening. This was all done while the 100 A DC current held the cores in reverse saturation, thus limiting the forces due to saturation, as well as mechanically controlling the assembly. This method proved successful and would be recommended for further applications with proper scaling for the device. Alternatively, for high power devices magnetization of the permanent magnets after assembly would be the optimal method.

4. Inductance Measurements

As explained above, the inductance as a function of current determines the effective operating range of the PMFCL.

Considering the parameters from Table 1, in the circuit configuration of the modeled grid in Figure 5, we can isolate the term for the differential voltage across the PMFCL device resulting with:

$$V_{PMFCL} = \frac{d}{dt}(LI). \quad (2)$$

Integrating both sides:

$$\int V_{PMFCL} dt = LI \rightarrow L_{(t)} = \frac{\int V_{PMFCL} dt}{I}. \quad (3)$$

Table 1. Parameters of Laboratory Modeled Grid.

Parameter	Value
Voltage rms [v]	230
Frequency [Hz]	50
Grid inductance, L_{grid} [mH]	4.578
Grid resistivity, R_{grid} [Ω]	0.415
Normal grid load, R_{Load} [Ω]	35

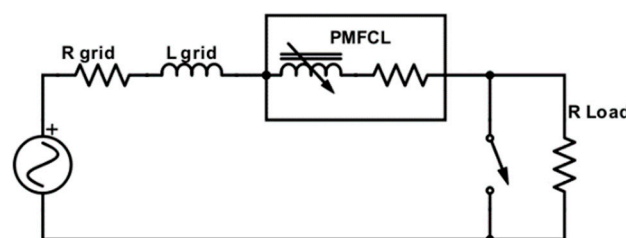


Figure 5. Modeled grid, schematics.

In the following, we first calculate $L(I)$ using Finite Element Method (FEM) analysis for optimizing the design prior to realization, and then measure the actual $L(I)$. The FEM simulations were designed to simulate the electrical circuit, while replacing the voltage source with a current source of a constant $\frac{dI}{dt}$, and calculating the voltage across the AC coils. This resulted in the voltage–current curve exhibited in Figure 6. The higher voltage values determine the effective range that the PMFCL has a high impedance and thus effectively limits the fault current. As a higher current is approached (around 120 A in Figure 6), the voltage decreases where we see again the result of the reversal in the direction of magnetization within the core, causing it to reenter the region of saturation in the opposite direction.

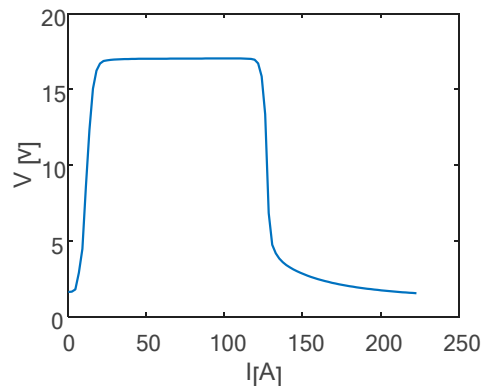


Figure 6. Voltage–current curve from FEM simulation analysis.

In order to do a real-time measurement of the current dependency of the inductance, L , we used a bank of super-capacitors with the equivalent capacitance of $C = 11.6 F$ to create a ramp-current function. The capacitors were chosen to provide a damping factor with $\zeta > 1$. The total AC coil resistance was 130 m Ω .

Figure 7 describes the voltage and current measured across the PMFCL, recreating similar conditions as used in the simulations. In the figure, we notice the voltage across the whole device starts at about 50 V due to the capacitors, with a zero-initial current. As the current rises from $I = 0$ to $I = 125 A$, the voltage across the device decreases almost linearly as the core exits its initial saturated state. This resulted in a high inductance and coupled with the slope of the current, this produced a high value of impedance (Equation (2)). The high impedance of the device in turn limits the immediate rise in current. At $t = 25$ the current reaches $\sim 120 A$, causing the core to enter its saturated region in the opposing direction due to the strong current, totally opposing the field created by the permanent magnets. The resulting decrease in inductance translates to a sharp decrease in voltage across the device, allowing the rising current to reach its maximum possible value in this configuration of around 200 A.

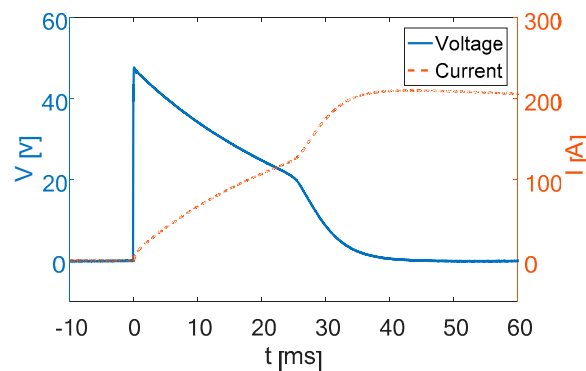


Figure 7. Discharge of capacitors' voltage compared to the current measured in the circuit.

Figure 8 compares the experimental current dependency of the inductance with that found in the simulations, as calculated from Equation (3). The initial values of the inductance proved a difficult measurement point, as taken from the first few microseconds in the discharging of the super-capacitors. By simulating a constant rise in the current, the initial value was calculated to be 0.73 mH . The initial measured current was zero however the circuitry involved in the switch caused a challenge to create an instantaneous smooth rise in the current. This likely caused the immediate rise in inductance from the initial measured value 1.06 mH to 1.3 mH at the 6 A point while the simulated inductance held a relatively steady value until the 6 A point. It is past this point that we expect the strong increase in the inductance as the device enters its fault mode. Indeed, past 6 A we find a significant increase in the inductance in both the simulation and the measurement.

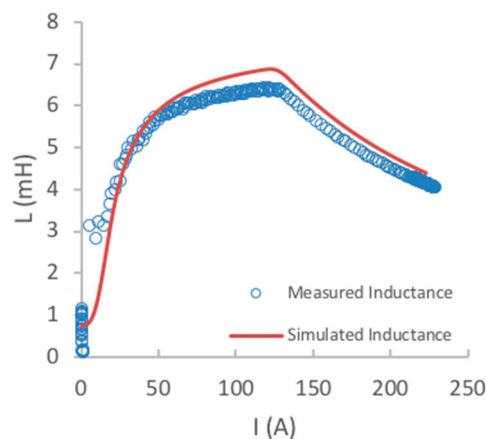


Figure 8. Comparison of simulated and measured inductance, L , as a function of current, I .

The measured and simulated curves are in qualitative agreement. We attribute the deviations between the curves to the non-ideal filling factor of the AC coils and the non-perfect magnet-core alignment of the realized model. This measurement holds essentially all of the data needed to define the effective current limiting regions for a specific SCFCL device. Adding this as a common method of analysis would greatly improve the comparison of PMFCL device capabilities compared to other modeling and measurement methods [23,24].

5. Nominal Measurements

Using the live circuit grid shown in Figure 5 with the values listed in Table 1, the voltage across the PMFCL was measured in real-time with the normal grid load values. The measurement (shown in Figure 9) resulted in a slight deviation from a clean sine wave, agreeing with the voltage source, with a 2% measured voltage drop across the device. The slight distortion of the sine wave is the result of a saturation somewhat lesser than designed for in the magnetic cores. As a result, each arm becomes slightly more saturated when the \vec{H}_{AC} produced and is aligned with the same direction of the permanent magnets' field. Then, the applied reverse field has a much smaller effect than if applied to an arm with the same previous direction of \vec{H}_{AC} . This explains the slight deviation in the peak amplitudes in the positive and negative directions, what may seem as a small DC-like component in the voltage.

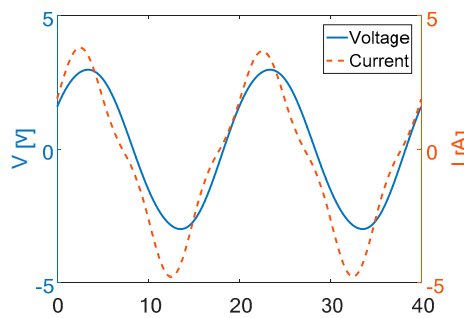


Figure 9. The time dependence of the voltage and current as measured in the nominal state.

6. Fault Measurements

The fault is modeled when the load of the grid is shorted (by means of the switch shown in Figure 5) with the total resistance going from a value of 35.5Ω to a value of 0.42Ω of the grid itself. This results in a total grid impedance of $\sim 1.5 \Omega$ which leads to a prospective fault current of $\sim 150 A_{rms}$.

Ideally, the limited current should be around 50% of the prospective current to provide a good limiting factor yet maintain the selectivity feature in the grid. The success of our design is visualized in Figure 10, where the fault current is shown as measured with and without the PMFCL connected. The results show a limited current of $73 A_{rms}$ which is in excellent agreement with the design target. Figure 11 shows the limited fault current compared to the voltage across the AC coils. The sharp fall in voltage near the maximum value of the waveform occurs due to the current passing through the zero value. At this point the core immediately returns to its saturated state, only to leave it once again as the current rises past the zero point. This voltage signal is characteristic for saturated core FCL devices as noted in [25]. These figures also illustrate the strength of the online PMFCL being in series with the circuit with no added active components.

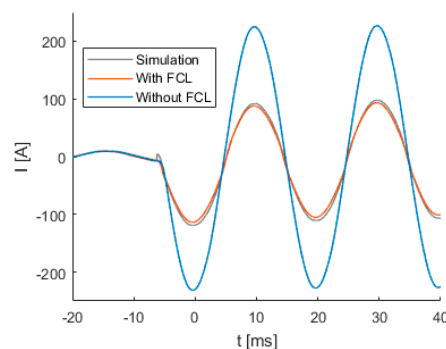


Figure 10. Fault current simulated and measured with/without PMFCL device as a function of time.

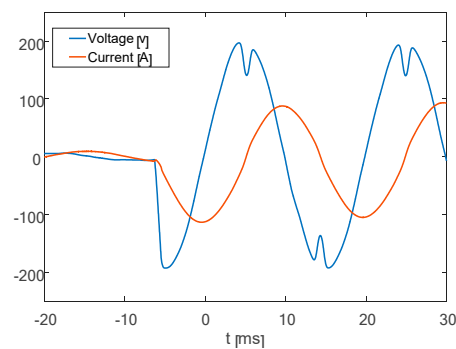


Figure 11. Fault voltage and current on PMFCL as a function of time.

7. Summary and Conclusions

This paper described a saturated cores PMFCL prototype design which exploits several concepts in improving the implementation of permanent magnets as magnetic field bias sources. A full simulation and live grid measurement analysis achieved satisfactory results, strengthening the methods of concepts discussed. Other than meeting the unique advantages that characterize PMFCLs, our novel concept marks several innovative approaches for improving the insertion impedance for nominal cycles. These include:

1. A closed magnetic path that eliminates multidirectional flux paths;
2. A large permanent magnet to core surface ratio to achieve optimal deep saturation throughout the cores;
3. Asymmetrical placement of the permanent magnets to decrease residual fields while increasing the weak center core point flux; and
4. Split AC coils to cancel the use of the weakest point on the cores.

This design improves the total efficiency as well as minimizing the amount of material to achieve the results. Conclusions can be made that properly incorporating these design attributes for future PMFCL devices will increase their efficiency and providing high power quality to the grid, while minimizing materials used, thus maximizing the performance and adoption of PMFCLs. The careful assembly and processes considered are a step forward in understanding the implications in building a PMFCL and similar methods should be used and modified for scaled up high voltage systems.

Author Contributions: Research and realization of this project is credited to the authors of this paper. Conceptualization, Y.N., S.W.; methodology, J.L., A.F.; software, J.L.; validation, Y.N., S.W. and Y.Y.; formal analysis, J.L., Y.N.; investigation, J.L.; resources, A.F., S.W.; data curation, J.L.; writing—original draft preparation, J.L.; writing—review and editing, S.W., Y.Y.; visualization, Y.N.; supervision, Y.Y.; project administration, S.W.; funding acquisition, Y.Y., S.W.

Funding: This research was funded by the Israeli Ministry of National Infrastructure, Energy, and Water Resources, Grant # 214-11-004.

Conflicts of Interest: The authors declare no conflict of interest.

References

1. Noe, M.; Steurer, M.; Eckroad, S.; Adapa, R. Progress on the R&D of fault current limiters for utility applications. In Proceedings of the 2008 IEEE Power and Energy Society General Meeting—Conversion and Delivery of Electrical Energy in the 21st Century, Pittsburgh, PA, USA, 20–24 July 2008; pp. 1–4.
2. Naeckel, O.; Noe, M. Design and Test of an Air Coil Superconducting Fault Current Limiter Demonstrator. *IEEE Trans. Appl. Supercond.* **2014**, *24*, 3. [[CrossRef](#)]
3. Cvoric, D.; de Haan, S.W.; Ferreira, J.A. Comparison of the four configurations of the inductive Fault Current Limiter. In Proceedings of the 2008 IEEE Power Electronics Specialists Conference 2008, Rhodes, Greece, 15–19 June 2008; pp. 3967–3973.
4. Moriconi, F.; De La Rosa, F.; Darmann, F.; Nelson, A.; Masur, L. Development and Deployment of Saturated-Core Fault Current Limiters in Distribution and Transmission Substations. *IEEE Trans. Appl. Supercond.* **2011**, *21*, 1288–1293. [[CrossRef](#)]
5. Alam, M.; Abido, M.; El-Amin, I. Fault Current Limiters in Power Systems: A Comprehensive Review. *Energies* **2018**, *11*, 1025. [[CrossRef](#)]
6. GridOn. Available online: <http://www.gridon.com/index.html> (accessed on 1 June 2018).
7. Nexans and AMSC. Superconductor Fault Current Limiters for MV AC Networks. 2018. Available online: <http://www.amsc.com/documents/superconductor-fault-current-limiters-for-mv-ac-networks/> (accessed on 3 August 2015).
8. Applied Materials. Available online: <http://www.appliedmaterials.com/technologies/fault-current-limiters> (accessed on 1 June 2018).
9. Raju, B.P.; Parton, K.C.; Bartram, T.C. A Current Limiting Device Using Superconducting D.C. Bias Applications and Prospects. *IEEE Trans. Power Appar. Syst.* **1982**, *PAS-101*, 3173–3177. [[CrossRef](#)]

10. Nikulshin, Y.; Wolfus, Y.; Friedman, A.; Yeshurun, Y. Dynamic Inductance in Saturated Cores Fault Current Limiters. *J. Supercond. Nov. Magn.* **2014**, *28*, 579–583. [[CrossRef](#)]
11. Mukhopadhyay, S.C.; Dawson, F.P.; Iwahara, M.; Yamada, S. Analysis, design and experimental results for a passive current limiting device. *Electr. Power Appl. IEE Proc.* **1999**, *148*, 513–519.
12. Iwahara, M.; Mukhopadhyay, S.C.; Yamada, S.; Dawson, F.P. Development of passive fault current limiter in parallel biasing mode. *IEEE Trans. Magn.* **1999**, *35*, 3523–3525. [[CrossRef](#)]
13. Hall, J.; Cheer, A. Fault current limiter surge protection device for the power grid based upon zero power consumption ceramic ferrite permanent magnets. In Proceedings of the 22nd International Conference and Exhibition on Electricity Distribution (CIRED 2013), Stockholm, Sweden, 10–13 June 2013.
14. Yuan, J.; Lei, Y.; Wei, L.; Tian, C.; Chen, B.; Du, Z. A Novel Bridge-Type Hybrid Saturated-Core Fault Current Limiter Based on Permanent Magnets. *IEEE Trans. Magn.* **2015**, *51*, 1–4.
15. Wei, B.C.L.; Tian, C.; Gao, Y.; Muramatsu, K.; Yuan, J. Optimization study of a novel small-section permanent-magnet-biased fault current limiter with leakage flux effect. In Proceedings of the 2016 IEEE Conference on Electromagnetic Field Computation (CEFC), Miami, FL, USA, 13–16 November 2016.
16. Wei, L.; Chen, B.; Yuan, J.; Tian, C.; Zhong, Y.; Li, X.; Gao, Y.; Muramatsu, K. Performance and Optimization Study of a Novel Compact Permanent-Magnet-Biased Fault Current Limiter. *IEEE Trans. Magn.* **2017**, *53*, 1–4. [[CrossRef](#)]
17. Yuan, J.; Zhong, T.; Lei, Y.; Tian, C.; Wei, L.; Guan, W.; Gao, Y.; Muramatsu, K.; Chen, B. A novel topology of hybrid saturated core fault current limiter considering permanent magnets stability performance. In Proceedings of the 2016 IEEE Conference on Electromagnetic Field Computation (CEFC), Miami, FL, USA, 13–16 November 2016.
18. Chen, B.; Wei, L.; Lei, Y.; Zhong, Y.; Tian, C.; Guan, W.; Gao, Y.; Muramatsu, K.; Yuan, J. Investigation on a modified hybrid compact saturated-core fault current limiter based on permanent magnets. In Proceedings of the 2016 IEEE Conference on Electromagnetic Field Computation (CEFC), Miami, FL, USA, 13–16 November 2016.
19. Hong-shun, L.; Liang, Z.; Li, Q.; Siew, W.H.; Yuan, M. Operating characteristics of the Permanent-Magnet-Biased Saturation Based Fault Current Limiter. In Proceedings of the 2008 International Conference on High Voltage Engineering and Application, Chongqing, China, 9–12 November 2008; pp. 503–507.
20. Liang, Z.; Qing-min, L.; Hong-shun, L.; Siew, W.H. Study on the feasibility of developing high voltage and large capacity permanent-magnet-biased fault current limiter. In Proceedings of the 2009 44th International Universities Power Engineering Conference (UPEC), Glasgow, UK, 1–4 September 2009; pp. 1–5.
21. Nikulshin, Y.; Wolfus, Y.; Friedman, A.; Yeshurun, Y. Improving the performance of saturated cores fault current limiters by varying winding density in the AC coils. *IEEE Trans. Appl. Supercond.* **2015**, *25*. [[CrossRef](#)]
22. World Health Organization (WHO). Static Electric and Magnetic Fields. Electromagnetic fields and public health. 2006. Available online: <http://who.int/peh-emf/publications/facts/fs299/en/> (accessed on 19 October 2018).
23. Yuan, J.; Lei, Y.; Tian, C.; Chen, B.; Yu, Z.; Yuan, J.; Zhou, J.; Yang, K. Performance Investigation of a Novel Permanent Magnet-Biased Fault-Current Limiter. *IEEE Trans. Magn.* **2015**, *51*. [[CrossRef](#)]
24. Wilson, P. Modeling the Non Linear Behavior of a Magnetic Fault Current Limiter. *Adv. Electromagn.* **2015**, *4*, 1–7. [[CrossRef](#)]
25. Nikulshin, Y.; Wolfus, Y.; Friedman, A.; Yeshurun, Y. Dynamic core length in saturated core fault current limiters. *Supercond. Sci. Technol.* **2013**, *26*. [[CrossRef](#)]

